

Effect of Mn doping on structural, dielectric and magnetic properties of BiFeO₃ thin films

S. Riaz · S. M. H. Shah · A. Akbar ·
S. Atiq · S. Naseem

Received: 23 January 2014 / Accepted: 28 July 2014 / Published online: 2 September 2014
© Springer Science+Business Media New York 2014

Abstract Bismuth iron oxide is amongst the class of materials that exhibit simultaneous presence of ferromagnetic and ferroelectric properties with potential applications in spintronic devices. However, there are some problems associated with BiFeO₃ including large leakage current, volatile nature of Bi₂O₃ along with weak ferromagnetic/antiferromagnetic behavior. In order to overcome these difficulties we here report the effect of manganese (Mn) doping on BiFeO₃ (BiFe_{1-x}Mn_xO₃ where $x = 0.0-0.3$, with interval of 0.05) thin films prepared using sol-gel and spin coating method. X-ray diffractometer (XRD) results show formation of phase pure rhombohedrally distorted perovskite structure. However, with the increase in Mn content, XRD peak positions shift to higher angle indicating reduction in lattice parameters and consequently the unit cell volume. Crystallite size in un-doped and Mn-doped BiFeO₃ films is below cycloidal spin arrangement of BiFeO₃, i.e. 62 nm. This along with charge compensation mechanism, arising due to replacement of trivalent cation with divalent ion, enhances the magnetic properties of BiFe_{1-x}Mn_xO₃ thin films. Ferromagnetic behavior instead of antiferromagnetic nature of BiFeO₃ is observed in these BiFe_{1-x}Mn_xO₃ thin films for all Mn concentrations. High saturation magnetization of 102 emu/cm³ was observed for Mn content of 0.2. Dielectric constant increases and the dielectric loss decreases as the dopant concentration is increased resulting in high dielectric constant and low dielectric loss at $x = 0.25$. The surface work function (wf) has been calculated using Scanning

Kelvin Probe technique. The wf results are correlated to the structural and then dielectric properties.

Keywords Sol-gel · Thin film · Ferromagnetism · BiFeO₃ · Manganese doping · Dielectric constant

1 Introduction

Amongst the new generation memory devices, Ferroelectric Random Access Memories (FeRAMs) have advantages over other non-volatile memories including low power consumption and high read-write capacity [1, 2]. For future FeRAMs the area of each cell must be reduced to increase the integration density. However, the polarization reversal current is reduced if the area of the capacitor is reduced thus making it difficult to store information using electric current. To overcome this difficulty development of new ferroelectric materials with high value of remnant polarization has become an essential part of today's research. Bismuth iron oxide (BiFeO₃; BFO) is a promising candidate because of its high remnant polarization. Bismuth iron oxide has rhombohedrally distorted perovskite structure with high antiferromagnetic Neel temperature and high ferroelectric Curie temperature. However, difficulties associated with bismuth iron oxide are: (1) large leakage current and (2) antiferromagnetic behavior of BiFeO₃. The large leakage current results in stability issues of BiFeO₃ whereas antiferromagnetic domains are rather difficult to read [1, 2]. In order to overcome these difficulties both A-site (Bi-substitution) and B-site (Fe-substitution) dopants have been reported in the literature including Ba [3], Ca [4], Co [5], Er [6] and Ni [7] etc. B-site doping is given special attention as the magnetic properties are much enhanced due to the replacement of Fe with transition

S. Riaz · S. M. H. Shah · A. Akbar · S. Atiq · S. Naseem (✉)
Centre of Excellence in Solid State Physics, University of the
Punjab, Lahore 54590, Pakistan
e-mail: shahzad_naseem@yahoo.com

A. Akbar
e-mail: aseya22@hotmail.com

metal due to the difference in magnetic moment of the two cations along with homogeneity in spin structure that arises as the consequence of doping. However, the extent of improvement is different in each study even if the dopant atom is the same. So, it is rather difficult to decide which dopant is the best for improvement of magnetic and electrical properties [4–9]. Moreover, magnetic properties reported in the case of even doped BiFeO₃ are still far beyond the industrial applications [8–10].

Mn has an oxidation states of 2+ to 4+, however, 2+ state is most stable state [11]. Manganese (Mn²⁺) is a potential doping candidate with ionic radius of 0.067 nm indicating an easy replacement with Fe³⁺ cations (ionic radius of 0.087 nm). In literature there are various reports regarding the replacement of Fe³⁺ with Mn²⁺ in BiFeO₃ but the dopant concentration range studied is rather limited [12, 13]. To date, various methods have been reported for synthesis of un-doped and doped bismuth iron oxide thin films including radio frequency (RF) sputtering [1], solid state precursor method [14], spray pyrolysis deposition [15], sol–gel method [3, 5], chemical combustion route [4], pulsed laser deposition [16] etc. Amongst these techniques sol–gel synthesis offers the advantages of being simple, low cost and vacuum free technique [17]. Kim et al. [1] prepared Bi_{1.1}Fe_{0.95}Mn_{0.05}O₃ thin films using RF sputtering and studied the ferroelectric properties. Reddy et al. [15] prepared Bi(Fe_{0.9}Mn_{0.1})O₃ thin films using spray pyrolysis technique and obtained saturation magnetization of 0.14 μ_B per formula unit. Sharma et al. [8] prepared Mn doped BiFeO₃ thin films using sol–gel method for 10–30 % dopant concentration and studied the optical properties of thin films. Gheorghiu et al. [9] prepared BiFe_{1-x}Mn_xO₃ ceramics for x = 0–0.3 by solid state reaction method and studied the dielectric properties. Tang et al. [10] prepared BiFe_{0.95}Mn_{0.05}O₃ thin films using chemical solution method and studied dielectric and magnetic properties. It has been previously reported by our research group that careful choice of solvent in sol–gel synthesis of bismuth iron oxide thin films helps in not only achieving pure phase of bismuth iron oxide at low temperature of 300 °C but also can lead to ferromagnetic behavior [18–20].

In the present study un-doped and Mn-doped (BiFe_{1-x}Mn_xO₃, x = 0.0–0.3) sols were synthesized by following the sol–gel route. Spin coated thin films were annealed in vacuum at 300 °C for 60 min in the presence of 500 Oe applied magnetic field (MF). Structural, magnetic, dielectric and surface work function (wf) properties have been correlated with the variation in Mn-doping concentrations.

2 Experimental details

Research grade iron nitrate (Fe(NO₃)₃·6H₂O, 99.9 % purity), bismuth nitrate (Bi(NO₃)₃·5H₂O, 99.5 % purity) and

manganese nitrate (Mn(NO₃)₃·6H₂O, 99.9 % purity) were used as precursors without further purification. For sol–gel process metal alkoxides are mostly used as precursors that have some downsides like high cost, toxic nature and high hydrolysis rate which makes it difficult to control the composition. Nitrates, as precursors, are cost effective due to their low decomposition temperatures as compared to other salts [21, 22]. The precursor solutions of bismuth and iron were prepared by dissolving Fe(NO₃)₃·6H₂O and 10 wt% excess of Bi(NO₃)₃·5H₂O separately in ethylene glycol. Bismuth and iron have different electronegativities (Fe ~ 1.83 and Bi ~ 2.03) that lead to different hydrolysis rates. Bismuth has a high hydrolysis rate as compared to iron so it becomes difficult to synthesize high quality sol. Excess 10 wt% bismuth was added to compensate the loss of bismuth oxide upon annealing. Ethylene glycol (OHC₂H₄OH) is a linearly structured molecule with two hydroxyl groups which helps to compensate for the difference in hydrolysis rates of bismuth and iron thus leading to the synthesis of a stable sol. Furthermore, it has been reported previously that choice of ethylene glycol as a solvent helps in not only achieving phase pure bismuth iron oxide at a lower temperature of 300 °C but also helps in achieving ferromagnetic behaviour [18–20]. Two solutions were prepared prior to the final sol synthesis as can be seen in Fig. 1. Solution 1 was prepared by dissolving iron nitrate in 30 ml ethylene glycol and stirred at room temperature for 30 min. Another solution (solution 2) was prepared by dissolving bismuth nitrate in ethylene glycol and stirred at room temperature for 30 min. Acidic nature, with pH 1, was observed for both of the solutions. The two solutions were mixed together and stirred at 60 °C for several hours to obtain BiFeO₃ sol. pH of the final sol was preserved to be 1. Solution 3 was prepared for doping purposes by dissolving Mn(NO₃)₃·6H₂O in ethylene glycol and stirred at room temperature for 30 min. Appropriate amounts of bismuth iron oxide sol and solution 3 were mixed together to obtain BiFe_{1-x}Mn_xO₃ sol with x = 0.0–0.3 with intervals of 0.05. Details of this sol–gel process can be seen in Fig. 1. The overall reactions are proposed in Eqs. 1–4. Shelf life of more than 1 year, without any precipitation or gelation, was observed for un-doped and Mn-doped sols. BiFe_{1-x}Mn_xO₃ sols were spin coated onto copper substrates at 3,000 rpm for 30 s using Delta 6RC spin coater. Before spin coating copper substrates were etched with diluted HCl followed by repeated rinsing in DI water. Substrates were then placed in ultrasonic bath in acetone and then IPA for 10 min each. Spin coated films were dried at room temperature and then annealed in vacuum in the presence of 500 Oe MF at 300 °C for 60 min.

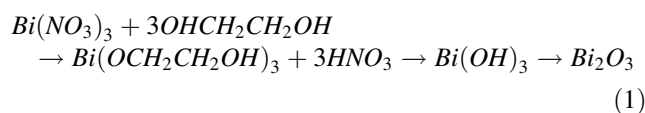
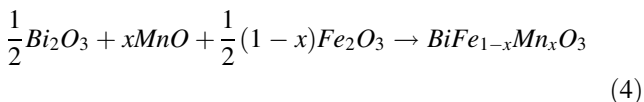
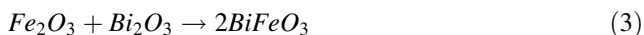
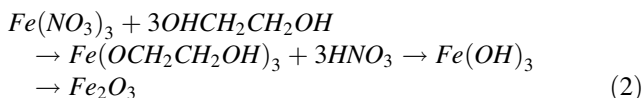
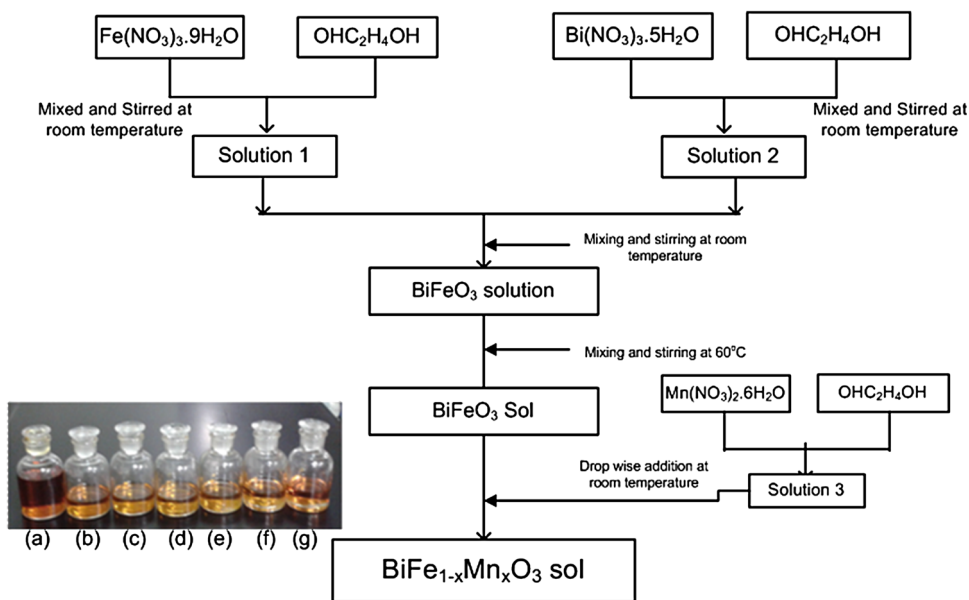


Fig. 1 Flow chart for the synthesis of $\text{BiFe}_{1-x}\text{Mn}_x\text{O}_3$ sols; inset shows sols synthesized by varying Mn content as *a* 0.0, *b* 0.05, *c* 0.1, *d* 0.15, *e* 0.2, *f* 0.25, *g* 0.3



$\text{BiFe}_{1-x}\text{Mn}_x\text{O}_3$ thin films were characterized structurally using Bruker D8 Advance XRD with Ni filtered CuK_α ($\lambda = 1.5406 \text{ \AA}$) radiations. Magnetic properties were studied using Lakeshore’s 7407 Vibrating Sample Magnetometer (VSM). Data was taken with a time constant of 0.3 s for 60 data points resulting in data acquisition time of approximately 10 min. Dielectric properties were studied using 6500B Precision Impedance Analyzer in parallel plate configuration. Surface wf measurements were performed using KP Technology’s Scanning Kelvin Probe system.

3 Results and discussion

Figure 2 shows XRD patterns of un-doped and Mn-doped BiFeO_3 thin films. Presence of diffraction peaks corresponding to (104), (110), (024) and (122) planes indicate the formation of phase pure rhombohedrally distorted perovskite structure (JCPDS card no. 86-1518). No peaks corresponding to non-perovskite bismuth rich $\text{Bi}_{35}\text{FeO}_9$ and bismuth deficient $\text{Bi}_2\text{Fe}_4\text{O}_9$ are observed even in case of un-doped BiFeO_3 thin films ($x = 0.0$). Non perovskite phases are suppressed by using 10 wt% excess of bismuth

that helps in compensating for the volatile nature of Bi_2O_3 during heat treatment. It is worth mentioning here that these films are annealed at rather low temperature of 300 °C. In the literature to the best of our knowledge there are so far no reports on crystallinity of BiFeO_3 films at 300 °C. Huang and Shannigrahi [23] reported pure BiFeO_3 films on Pt/Ti/Si/SiO₂ substrate in the temperature range of 400–500 °C using chemical solution deposition method. Sharma et al. [8] prepared nanostructured BiFeO_3 thin films on glass substrate via sol–gel and obtained crystalline BiFeO_3 phase upon annealing at 450 °C. Huang et al. [24] obtained crystalline phase on Si and LaNiO_3/Si after crystallizing the films at 600 °C. Das et al. [25] used wet chemical route and obtained the required phase after annealing the films at 400 and 500 °C. Zhang et al. [26] obtained polycrystalline BiFeO_3 thin films, prepared via chemical solution deposition method, upon annealing at 500 °C.

In the XRD patterns of Fig. 2, no peaks corresponding to manganese oxide are observed even at high dopant concentration of 0.3 indicating that the dopant has been successfully incorporated into the host lattice. The ratio of ionic radii of Mn^{2+} and Bi^{3+} is 0.8. This value is higher than 0.59 that is the criterion for synthesis of interstitial solid solution [27]. Therefore, it is difficult for manganese ions to occupy interstitial sites rather it will replace Fe^{3+} ions on the substitutional sites. Shift in the peak positions to relatively higher diffraction angles was observed with the increase in dopant concentration. This shift might have been observed because of the slightly lower ionic radii of Mn^{2+} as compared to Fe^{3+} .

Crystallite size, strain induced, and texture coefficient were calculated using Eqs. 5–7 [27–29]. Crystallite size

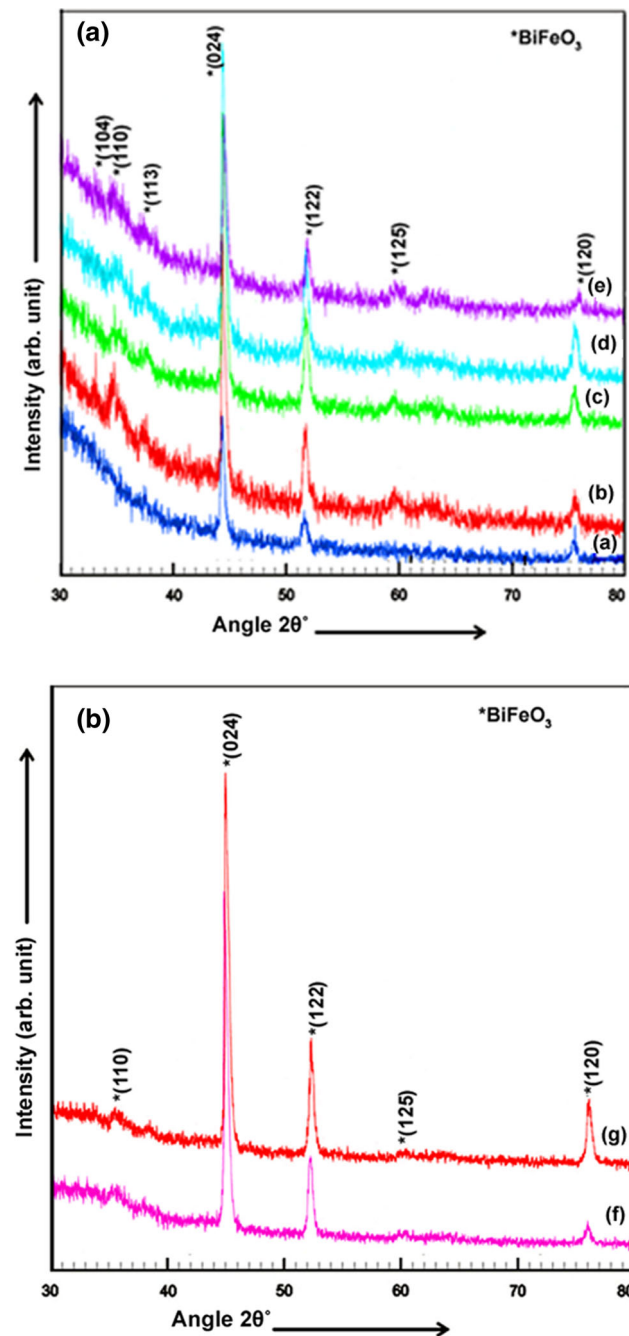


Fig. 2 XRD patterns of $\text{BiFe}_{1-x}\text{Mn}_x\text{O}_3$ thin films by varying Mn content ‘x’ as a 0.0, b 0.05, c 0.1, d 0.15, e 0.2, f 0.25 and g 0.3

and crystallinity of thin films is plotted as a function of dopant (Mn) concentration in Fig. 3a. Decrease in crystallite size from 23 to 17 nm was observed with the increase in Mn content from 0.0 to 0.3. During sol-gel synthesis, the crystallite size strongly depends on the rate of nucleation. Addition of Mn content in bismuth iron oxide sol generates localized heating around the ions that take part in substitution mechanism of smaller Mn^{2+} ionic

radius with larger Fe^{3+} cations [11]. As a result of which a temperature gradient is established in the solution and the intrinsic temperature is localized around the ions. This temperature gradient and localized heating delays the Ostwald ripening mechanism [30–32] thus decreasing the crystallite size with increase in Mn dopant concentration. Furthermore, grain growth in thin films depends on: (1) neighboring grains with different energies due to the curvature of energetic grain boundaries and (2) different amounts of accumulated strain energies [29]. Variation in strain produced and texture coefficient, as a function of dopant concentrations, is shown in Fig. 3b, c.

$$t = \frac{k\lambda}{B\cos\theta} \quad (5)$$

$$\text{Strain} = \frac{\Delta d}{d} = \frac{d_{\text{exp}} - d_{\text{hkl}}}{d_{\text{hkl}}} \quad (6)$$

$$T_{c(\text{hkl})} = \frac{I_{(\text{hkl})}/I_{o(\text{hkl})}}{\left(\frac{1}{N}\right)\sum I_{(\text{hkl})}/I_{o(\text{hkl})}} \quad (7)$$

where, k is the shape factor taken as 0.9, λ is the wavelength, B is Full Width at Half Maximum (FWHM) and θ is the diffraction angle. $I_{(\text{hkl})}$ is the measured relative intensity of (hkl) plane, $I_{o(\text{hkl})}$ is the standard intensity of plane (hkl) taken from JCPDS card no. 86-1518, N is the number of diffraction peaks.

The lattice parameters and unit cell volume of the films were determined and then refined using Powder Cell Software, and are shown in Fig. 4a. Refined data obtained using “Powder Cell” software is given in Table 1. Lattice parameters (a and c) decrease with the increase in Mn concentration that is in accordance with Vegard’s law [27]. The decrease of lattice parameter with increasing manganese concentration in host BiFeO_3 lattice is due to small ionic radii of Mn^{2+} (0.067 nm) as compared to Fe^{3+} (0.087 nm) thus leading to contraction of unit cell as can be seen in Fig. 4b. Decreased unit cell volume consequently increases the density of films (Fig. 4b). High density values ($7.79\text{--}8.136\text{ g cm}^{-3}$) of the films for the entire concentration range indicates a compact structure. The increase in X-ray density is because of the increase in packing density of the films with replacement of Mn^{2+} with Fe^{3+} . Results presented in Figs. 2, 3, 4 show that Mn doping did not alter the crystal structure. However, generating an impact on cell parameters that in turns can affect the dielectric and magnetic properties of $\text{BiFe}_{1-x}\text{Mn}_x\text{O}_3$ thin films.

Dielectric properties of un-doped and Mn-doped BiFeO_3 thin films were studied using impedance analyzer in parallel plate configuration. Parallel capacitance and resistance were measured and then dielectric constant ‘ ϵ ’ and dielectric loss (tangent loss) ‘ $\tan \delta$ ’ were calculated using Eqs. 8, 9.

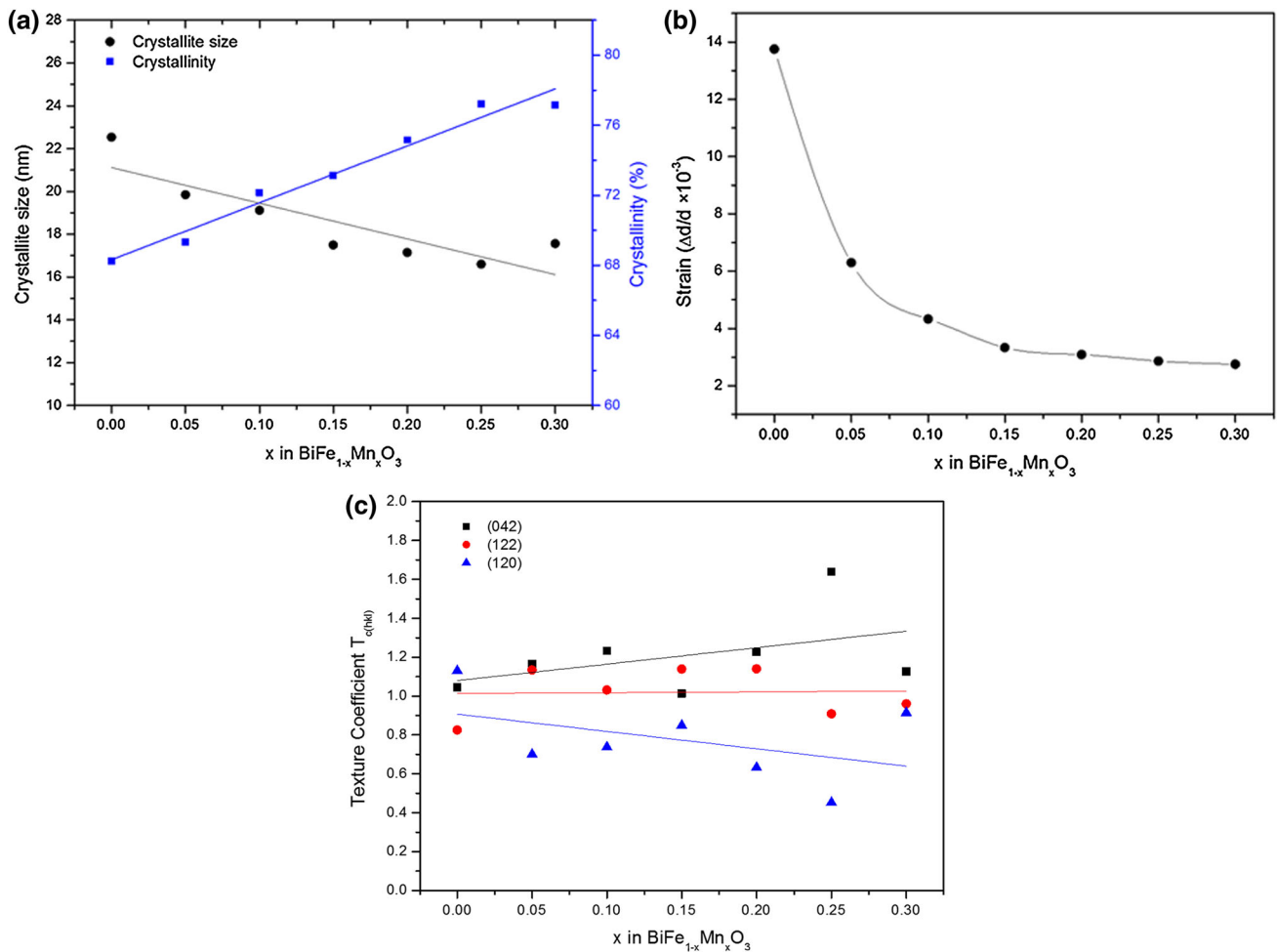


Fig. 3 Effect of Mn concentration on **a** crystallite size and crystallinity, **b** strain induced and **c** texture coefficient of thin films

$$\epsilon = \frac{C \times d}{\epsilon_o \times A} \tag{8}$$

$$\tan \delta = \frac{1}{2\pi\epsilon\epsilon_o\rho} \tag{9}$$

where, *C* is the capacitance, *d* is thickness of the specimen, *A* the area of the device, ϵ_o is the permittivity of free space and ρ is the resistivity of thin films. The dielectric constant and tangent loss, plotted in Fig. 5 as a function of frequency, decreases as the frequency increases and becomes constant at high frequencies showing normal dispersion behavior for all concentrations (i.e. $x = 0.0\text{--}0.3$). The dispersion in dielectric constant occurs due to the time required by the carriers to get align in the direction of field. At high frequencies the field reversal is so high that the carriers do not get enough time to get aligned in the direction of field [33]. Variation of dielectric tangent loss with frequency can be explained on the basis of Maxwell–Wagner two-layered model according to which the specimen is comprised of two layers, i.e. grains and grain

boundaries. Grains have low resistivity whereas the grain boundaries are more resistive [34]. The grains are more active at high frequencies whereas the grain boundaries become active at low frequencies resulting in decreased dielectric loss with the increase in frequency. Bhushan et al. [33] observed decrease in dielectric constant with increase in frequency and have reported dielectric constant values of 45.5, 31.4, 18.8 and 4.5 for un-doped and Ba-, Sr- and Ca-doped BiFeO₃. Verma et al. [34] also observed decrease in dielectric constant with increase in frequency from 50 to 1,000 Hz.

The dielectric constant and tangent loss are plotted as a function of dopant concentration in Fig. 6. For higher frequencies of 5–50 kHz, dielectric constant (ϵ) increases with the increase in dopant concentration up to $x = 0.2$ along with slight variation in ϵ from 0.1 to 0.2 particularly for 5 and 10 kHz. However, magnified effect of such variation was observed at lower frequencies of 1–2 kHz. These variations might have appeared because of the pronounced effect of electrode polarization along with the

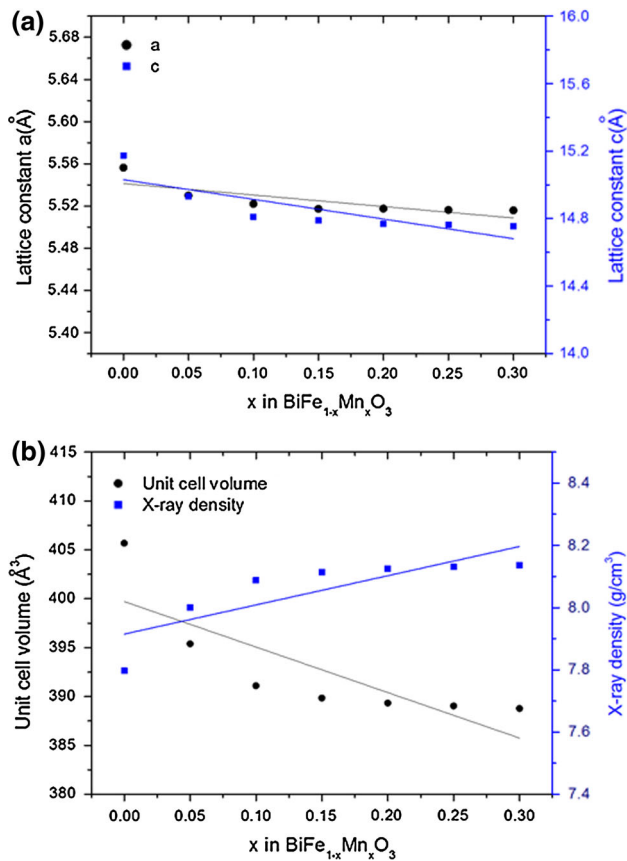


Fig. 4 **a** Lattice parameters a (Å) and c (Å) and **b** unit cell volume and X-ray density as a function of dopant concentration

sample at lower frequencies [35, 36]. For dopant concentration of 0.25, a remarkable increase in ϵ was observed at all frequencies and afterwards a decreasing trend was observed with further increase in dopant concentration to 0.3 (Fig. 6a).

At 10 and 50 kHz, un-doped sample showed dielectric constant (ϵ) value of ~ 4 and 2, respectively. However, a remarkable increase in ϵ (~ 84 at 10 kHz and ~ 80 at 50 kHz) was observed with the increase in Mn dopant concentration to 0.25. With further increase in Mn content to 0.3 ϵ reduced to ~ 40 at 10 and 50 kHz. Dielectric constant of thin films comes from both intrinsic and extrinsic parameters including (1) film orientation, (2) crystallite/grain size, (3) grain boundaries, (4) stresses, (5) crystal field and (6) domain wall pinning etc. Crystal field associated with surface bonds changes with the decrease in crystallite/grain size thus changing the dielectric constant [34]. Moreover, domain wall mobility also contributes towards the changes in dielectric properties. In the present study, increase in ϵ from 4 to 84, with the increase in dopant concentration to 0.25, might be attributed to decrease in crystallite size from 23 to 16 nm. Decrease in crystallite size increases the grain boundaries hindering the hopping process between the different states and grains [33, 34]. This results in accumulation of Mn^{2+} ions at the grain boundaries. This accumulation of cations increases the resistance and ultimately the dielectric constant values. Similar electronic behavior has been observed in the results

Table 1 Refined cell parameters of Mn doped BiFeO_3 thin films obtained using Powder Cell software

Mn content in $\text{BiFe}_{1-x}\text{Mn}_x\text{O}_3$	Input parameters				Output parameters				
	h	k	l	$2\theta^\circ$	d-spacing (Å)	Standard deviation in 2θ	RMS error	a (Å)	c (Å)
0.0	0	2	4	44.560	2.0317	0	2×10^{-8}	5.556195	15.17401
	1	2	2	51.640	1.7686				
0.05	0	2	4	44.940	2.0154	6×10^{-6}	1×10^{-8}	5.52976	14.93115
	1	2	2	51.940	1.7591				
0.1	0	2	4	45.10	2.0087	8×10^{-6}	2×10^{-8}	5.521923	14.81096
	1	2	2	52.040	1.7559				
0.15	0	2	4	45.150	2.0066	6×10^{-6}	1×10^{-8}	5.517206	14.78854
	1	2	2	52.090	1.7544				
0.2	0	2	4	45.170	2.0057	2×10^{-6}	1×10^{-8}	5.51743	14.76791
	1	2	2	52.095	1.7542				
0.25	0	2	4	45.18	2.0053	8×10^{-6}	5×10^{-8}	5.516202	14.76343
	1	2	2	52.105	1.7539				
0.3	0	2	4	45.19	2.0049	8×10^{-6}	1×10^{-8}	5.515864	14.75551
	1	2	2	52.110	1.7537				

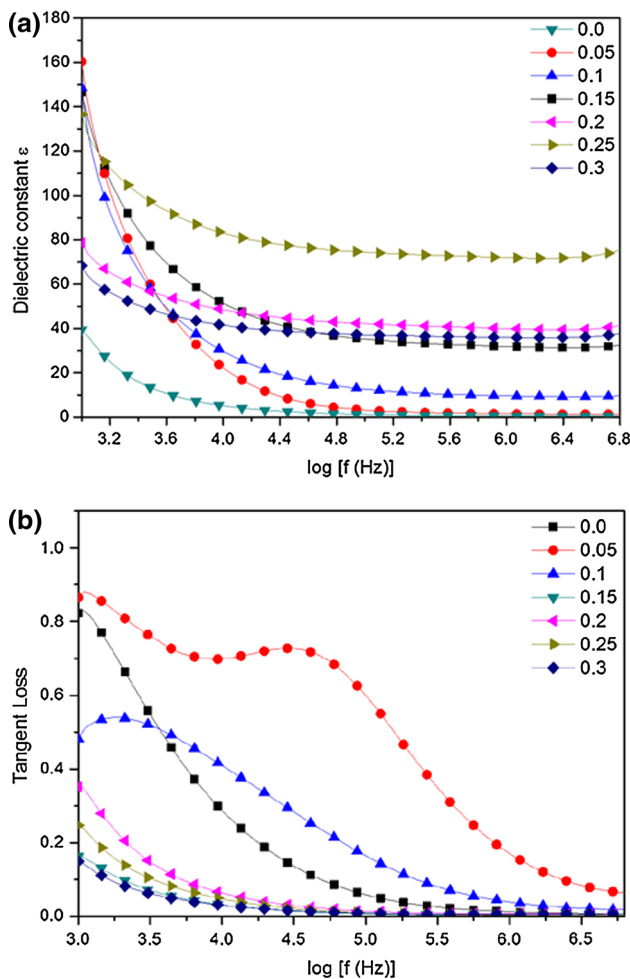


Fig. 5 **a** Dielectric constant, **b** tangent loss for $\text{BiFe}_{1-x}\text{Mn}_x\text{O}_3$ thin films

obtained using surface work function (wf) measurements. Minimum amount of energy required to remove an electron from the surface, with zero kinetic energy (K.E.), to a point just outside the material is known as wf of that material [37]. The required energy depends on optical, chemical, mechanical and electric characteristics of the region through which electron has to move. Therefore, wf is characteristic of any material and indicator of surface condition. The surface potential or wf of a sample can be measured with different techniques such as (1) Kelvin Probe, (2) photoelectron spectroscopy (PES) and (3) scanning electron microscopy (SEM) with electron beam induced current (EBIC) [38].

Kelvin probe method is an indirect technique, i.e., electrons are not extracted directly from the surface, instead using a reference surface (a vibrating tip) as the counter electrode the surface under study forms one plate of a parallel plate capacitor. The wf difference is determined by the addition of an external voltage termed as the backing potential (V_b) [38]. Figure 7 shows scanning Kelvin measurements showing wf of un-doped ($x = 0$) and

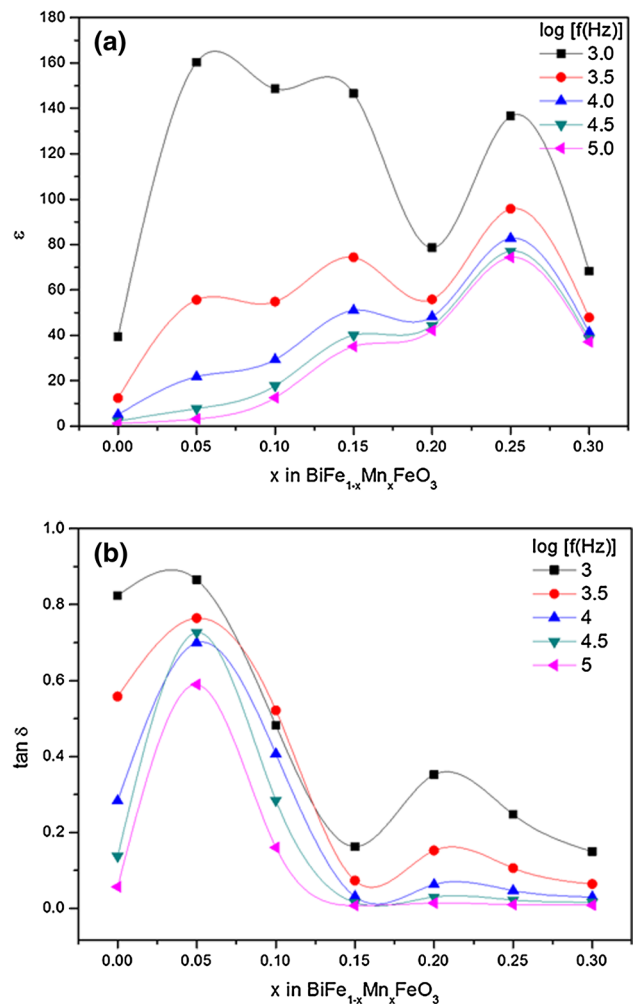
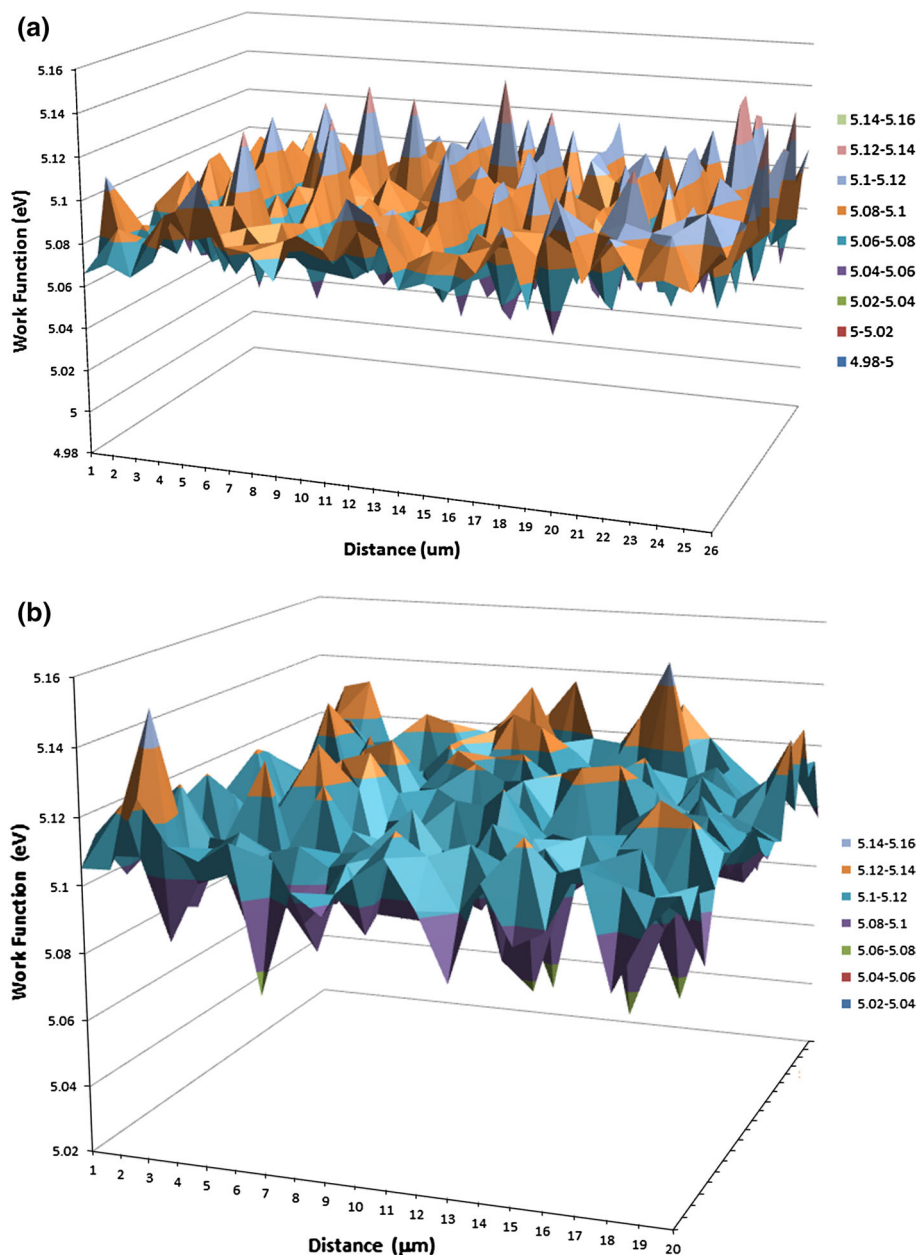


Fig. 6 **a** Dielectric constant, **b** tangent loss for as a function of dopant concentration

Mn-doped ($x = 0.3$) in (a) and (b) respectively. The average wf comparison of the 2 films shows that Mn-doped material has higher wf (5.12–5.14 eV) as compared to the un-doped one (5.08–5.1 eV). This clearly strengthens the postulate of increased dielectric strength due to reduced carrier concentration. Although, detailed research into use of Scanning Kelvin Probe Microscopy for investigating the effect of various sample preparation steps on the surface properties is underway, further deliberation into these figures indicates that grains and grain boundaries have different wf values. This strengthens our previous discussion of replacements and effects of Mn^{2+} and Fe^{3+} .

Increase in dielectric loss ($\tan \delta$) was observed at frequencies of 5–50 kHz up to dopant concentration of 0.05. A remarkable decrease in dielectric loss was observed with the increase in dopant concentration to 0.15 at all the frequencies (Fig. 6b). The dielectric loss remained almost constant at higher frequencies (5–50 kHz) with further increase in dopant concentration to 0.3 along with small

Fig. 7 Work function of **a** un-doped ($x = 0.0$) and **b** Mn-doped ($x = 0.3$) BiFeO₃ thin films



variations at 5 and 10 kHz. Such variations have been magnified at lower frequencies of 1–2 kHz. Doping of Mn in BiFeO₃ introduces oxygen vacancies due to charge compensation mechanism and increases the probability of electron hopping which results in dielectric loss [39, 40]. These increased dielectric values have been correlated to structural changes that are indicative of large number of grain boundaries and Mn doping effects.

Figure 8 shows M–H curves for un-doped and Mn-doped BiFeO₃ thin films. Un-doped BiFeO₃ films show ferromagnetic behavior as opposed to antiferromagnetic nature of the bulk BiFeO₃. Presence of open hysteresis (Fig. 8a) in un-doped BiFeO₃ films indicates the formation of ferromagnetic domains. As a result, spin orbit coupling

canting between two adjacent planes produces uncompensated magnetic moment of Fe³⁺ cations which is the cause of ferromagnetic behavior [41]. The uncompensated magnetic moment seems to have appeared during sol's synthesis [42] since in our case even un-doped films show ferromagnetic behaviour. It can be seen in Fig. 8b that Mn addition strongly affects the magnetic properties of BiFeO₃ films with the increase in saturation magnetization (M_s) up to 102 emu/cm³. Origin of ferromagnetic properties in otherwise antiferromagnetic BiFeO₃ lies in nanorange crystallite size of BiFeO₃ as observed in Fig. 3 i.e. crystallite size of 23–17 nm of BiFe_{1-x}Mn_xO₃ thin films. Helical spin structure of BiFeO₃, responsible for antiferromagnetic behavior, is suppressed with the decrease in

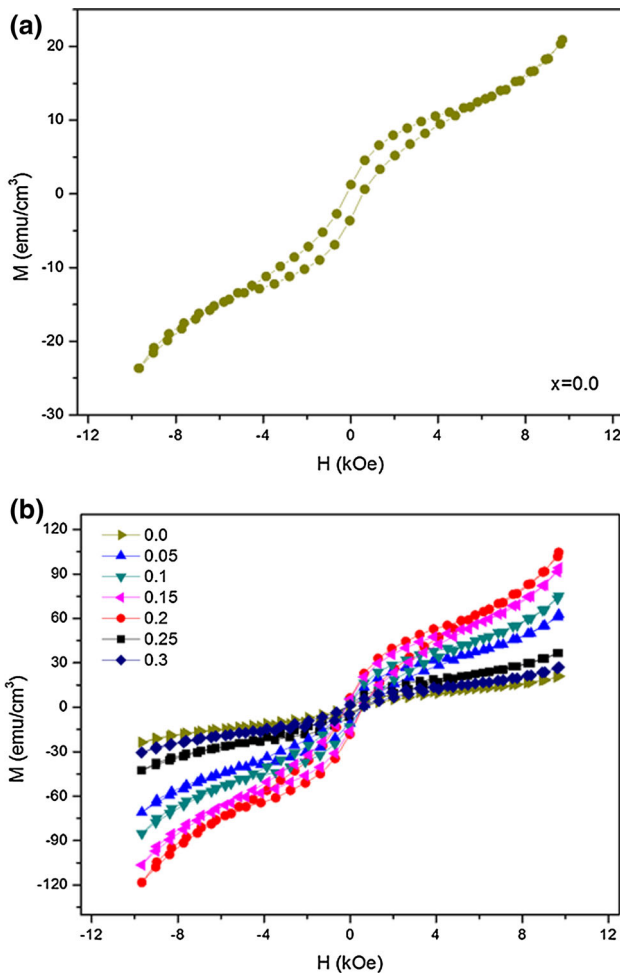


Fig. 8 Room temperature M–H curves for **a** un-doped and **b** Mn-doped BiFeO₃ thin films

crystallite size. The helical spin structure of BiFeO₃ has a periodicity of 62 nm with canting spin structure between the two consecutive ferromagnetic planes. The short-range magnetic ordering of un-doped bismuth iron oxide is G-type antiferromagnetic [2]. In this case each Fe³⁺ spin is enclosed by six neighboring spins that are antiparallel [2]. However, the alignment is not perfectly antiparallel. There is a canting moment that arises due to magnetoelectric coupling. However, there is also a long range structure that is composed of unequal spins of antiferromagnetically ordered sublattice. This cycloid has a repeat distance of 62 nm [2]. As manganese content is increased the distortion is created in the spiral spin structure with the decrease in crystallite size. Such distortion leads to conversion of helical arrangement to linear structure thus increasing the magnetic properties [12, 13]. In addition, by replacing a trivalent cation with divalent cation requires charge compensation mechanism that results in the formation of oxygen vacancies and/or conversion of Fe³⁺ cations to

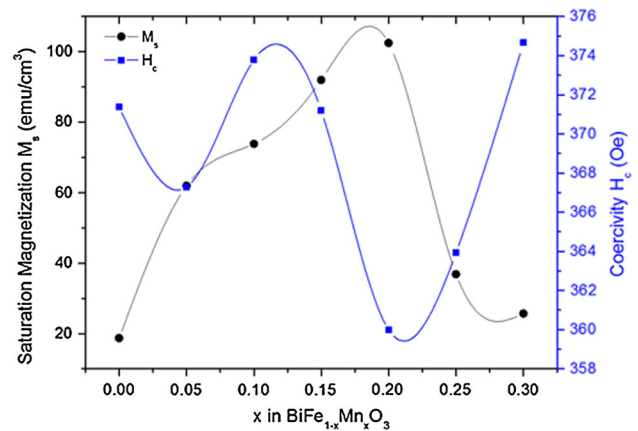


Fig. 9 Saturation magnetization and coercivity as a function of dopant concentration

Fe⁴⁺ cations. The presence of Fe⁴⁺ cations also enhances the ferromagnetic behavior of un-doped BiFeO₃ [43].

The ferromagnetic nature of BiFeO₃ films increases with manganese incorporation. The saturation magnetization increases to 102 emu/cm³ at x = 0.2, whereas further increase in Mn content decreases the magnetic moment. These results are in agreement with the values of dielectric constant given in Fig. 6a. A dip in dielectric constant values, at almost all frequencies, was observed for 0.2 Mn content. This dip is indicative of the presence of relatively larger carrier concentration reducing the dielectric constant. Variation in saturation magnetization (M_s) and coercivity (H_c) as a function of Mn dopant concentration is shown in Fig. 9.

The ferromagnetic behavior reported here is much enhanced as compared to that reported in the literature. Huang et al. [12] did not achieve considerable enhancement in magnetic properties (i.e. 2 emu/cm³ for x = 0.1) with Mn doping in BiFeO₃ thin films prepared by chemical solution deposition method and annealed at 600 °C. Basu et al. [13] observed considerable enhancement in magnetization (i.e. 2.75 emu/g) in Mn-doped BFO at low temperature of 10 K. Tang et al. [10] obtained ferromagnetic behavior in 5 % Mn doped BiFeO₃ with saturation magnetization of ~1 emu/cm³. Ahmed et al. [44] obtained antiferromagnetic behavior of un-doped bismuth iron oxide films and observed enhancement of magnetization with increase in lanthanum content to 0.3. Jangid et al. [45] observed antiferromagnetic behavior in undoped BiFeO₃ specimen and observed ferromagnetic hysteresis at dopant concentration of 50 %. Antiferromagnetic behavior in un-doped bismuth iron oxide thin films is also reported by Chaudhuri and Mandal [46]. Liu et al. [47] obtained saturation magnetization of 22.86 emu/cm³ with 0.5 % doping of titania in BiFeO₃. Habouti et al. [48] reported saturation

Table 2 Saturation magnetization of Mn doped BiFeO₃ thin films

Present work BiFe _{1-x} Mn _x O ₃		Literature	
x	M _s (emu/cm ³)		M _s (emu/cm ³)
0.0	18.7	BiFe _{0.95} Mn _{0.05} O ₃ [13]	~ 1
0.05	61.95		
0.1	73.86	Mn doped (5 %) BiFeO ₃ [14]	6.5
0.15	91.99	BiFe _{0.90} Mn _{0.10} O ₃ [12]	2
0.2	102.461		
0.25	36.838		
0.3	25.686		

magnetization of 30 emu/cm³ for un-doped BFO films. A comparison of the saturation magnetization observed in the present work with the previously reported values for Mn-doped BiFeO₃ is given in Table 2.

4 Summary

Un-doped and Mn-doped BiFeO₃ (BiFe_{1-x}Mn_xO₃; x = 0.0–0.3 with intervals of 0.05) thin films were prepared using sol–gel method. Ethylene glycol was used as a solvent. Films were annealed in vacuum at 300 °C for 60 min with 500 Oe applied MF. XRD patterns showed the formation of phase pure rhombohedrally distorted perovskite structure. It has been shown that incorporation of dopant causes changes in unit cell due to the smaller ionic radii as compared to that of iron. However, no peaks corresponding to MnO were observed indicating that dopant has been successfully incorporated into the host lattice. Dielectric constant of 84 at 10 kHz was observed for 0.25 Mn concentration. The high dielectric constant values have been correlated to large number of grain boundaries and due to Fe³⁺ replacement with Mn²⁺. These facts were consolidated with the variations in wf. BiFe_{1-x}Mn_xO₃ films showed ferromagnetic behavior, even in the un-doped sample as opposed to the antiferromagnetic nature of BiFeO₃. High value of saturation magnetization (102 emu/cm³) was observed for Mn content of 0.2.

References

- Kim JH, Funakubo H, Sugiyama Y, Ishiwara H (2011) *Curr Appl Phys* 11:S228–S231
- Catalan G, Scott JF (2009) *Adv Mater* 21:2463–2485
- Luo L, Luo W, Yuan G, Wei W, Yuan X, Zhang H, Shen K, Xu M, Xu Q (2013) *J Supercond Nov Magn* 26:3309–3313
- Tirupathi P, Chandra A (2013) *J Alloy Compd* 564:151–157
- Peng L, Deng H, Tian J, Ren Q, Peng C, Huang Z, Yang P, Chu J (2013) *Appl Surf Sci* 268:146–150
- Zhao J, Liu S, Zhang W, Liu Z, Liu Z (2013) *J Nanopart Res* 15:1969
- Zhao J, Zhang X, Liu S, Zhang W, Liu Z (2013) *J Alloy Compd* 557:120–123
- Sharma HB, Singh NB, Devi KN, Lee JH, Singh SB (2014) *J Alloy Compd* 583:106–110
- Gheorghiu F, Curecheriu L, Ianculescu A, Calugaru M, Mitoseriu L (2013) *Scripta Mater* 68:305–308
- Tang X, Dai J, Zhu X, Sun Y (2013) *J Alloy Compd* 552:186–189
- Gupta S, Tomar M, Gupta V (2013) *J Exper Nanosci* 8:261–266
- Huang JZ, Wang Y, Lin Y, Li M, Nan CW (2009) *J Appl Phys* 106:063911
- Basu S, Hossain SM, Chakravorty D, Pal M (2011) *Curr Appl Phys* 11:976–980
- Wang L, Xu JB, Gao B, Chang AM, Chen J, Bian L, Song CY (2013) *Mater Res Bullet* 48:383–388
- Reddy VA, Pathak NP, Nath R (2013) *Solid State Commun* 171:40–45
- Gao GY, Yang ZB, Huang W, Zeng HZ, Wang Y, Chan HLW, Wu WB, Hao JH (2013) *J Appl Phys* 114:094106
- Brinker CJ, Scherer GW (1990) *Sol–gel science—the physics and chemistry of sol–gel processing*. Academic Press, USA
- Shah SMH, Riaz S, Akbar A, Atiq S, Naseem S (2014) *IEEE Trans Magn*. doi:10.1109/TMAG.2014.2309720
- Shah SMH, Akbar A, Riaz S, Atiq S, Naseem S (2014) *IEEE Trans Magn*. doi:10.1109/TMAG.2014.2310691
- Riaz S, Shah SMH, Akbar A, Kayani ZN, Naseem S (2014) *IEEE Trans Magn*. doi:10.1109/TMAG.2014.2313002
- Xu JH, Ke H, Jia DE, Wang W, Zhou Y (2009) *J Alloy Compd* 472:473–477
- Brinker CJ, Scherer GW (1990) *Sol–gel science*. Academic Press, San Diego
- Huang A, Shannigrahi SR (2011) *Thin Solid Films* 519:4793–4797
- Huang D, Deng H, Yang P, Chu J (2010) *Mater Lett* 64:2233–2235
- Das S, Basu S, Mitra S, Chakravorty D, Mondal BN (2010) *Thin Solid Films* 518:4071–4075
- Zhang H, Chen X, Wang T, Wang F, Shi W (2010) *J Alloys Compd* 500:46–48
- Cullity BD (1956) *Elements of X-ray diffraction*. Addison-Wesley Publishing Company, USA
- Chen HL, Lu YM, Hwang WS (2005) *Mater Trans* 46:872–879
- Riaz S, Naseem S (2007) *J Mater Sci Technol* 23:499–503
- Acharya S, Singh K (2011) *Appl Nanosci* 1:97–101
- Phani AR, Santucci S (2006) *J Non Crystall Solid* 352:4093–4100
- Phani AR, Passacantando M, Santucci S (2007) *J Phys Chem Solid* 68:317–323
- Bhushan B, Basumallick A, Bandopadhyay SK, Vasanthacharya NY, Das D (2009) *J Phys D Appl Phys* 42:065004
- Verma KC, Ram M, Singh J, Kotnala RK (2011) *J Alloy Compd* 509:4967–4971
- Ishai PB, Talary MS, Caduff A, Levy E, Feldman Y (2013) *Meas Sci Technol* 24:102001
- Atia BS, Neha, Prakash J, Kumar R, Tripathi SK, Thakur N (2013) *J Nano Electron Phys* 5:19
- Satyam M, Ramkuma K (1990) *Foundations of electronic devices*. New Age International, Delhi
- Sadewasser S, Glatzel T (2012) *Kelvin probe force microscopy: measuring and compensating electrostatic forces*. Springer, Berlin
- Chauhan S, Arora M, Sati PC, Chhoker S, Katiyal SC, Kumar M (2013) *Ceram Inter* 39:6399–6405
- Sen K, Singh K, Gautam A, Singh M (2012) *Ceram Int* 38:243–249

41. Akbar A, Riaz S, Ashraf R, Naseem S (2014) IEEE Trans Magn. doi:[10.1109/TMAG.2014.2311826](https://doi.org/10.1109/TMAG.2014.2311826)
42. Riaz S, Naseem S, Xu YB (2011) J Sol-Gel Sci Technol 59:584–590
43. Chauhan S, Kumar M, Chhoker S, Katyal SC, Singh H, Jewariya M, Yadav KL (2013) Solid State Commun 152:525–529
44. Ahmed T, Vorobiev A, Gevorgian S (2012) Thin Solid Films 520:4470–4474
45. Jangid S, Barbar SK, Bala I, Roy M (2012) Phys B 407:3694–3699
46. Chaudhuri A, Mandal K (2012) Mater Res Bull 47:1057–1061
47. Liu YQ, Zhang J, Wu YH, Zhang YJ, Wei MB, Yang JH (2013) J Sol Gel Sci Technol 67:1–7
48. Habouti S, Solterbeck CH, Souni ME (2007) J Sol Gel Sci Technol 42:257–263